

Article

Ultrathin and Optically Transparent Microwave Absorber Based on Flexible Silver Nanowire Film

Yanfei Dong ¹ , Dingwang Yu ^{1,2}, Guochao Li ^{1,*}, Yulin Cao ¹, Youde Ruan ¹ and Mingtuan Lin ²

¹ Industries Training Centre, Shenzhen Polytechnic (SZPT), Shenzhen 518055, China; dongyanfei@szpt.edu.cn (Y.D.); ydw13049059@163.com (D.Y.); caoyulin@szpt.edu.cn (Y.C.); ruyude01@szpt.edu.cn (Y.R.)

² College of Electronic Science, National University of Defense Technology, Changsha 410073, China; linmingtuan08@nudt.edu.cn

* Correspondence: liguochao@szpt.edu.cn

Abstract: The design of an optically transparent and flexible metamaterial absorber was presented and fabricated. For this purpose, we use two different patterned silver nanowire films separated by the space layer, forming a transparent sandwiched structure with an ultrathin thickness. By analyzing the equivalent circuit model and distribution of electric field and current, the absorption physical mechanism has been theoretically investigated. The results show that the structure can achieve above 0.8 absorptions from 6 GHz to 18 GHz, and at the same time, this absorber also can obtain wide-angle property. The optical transmittance of the fabricated absorber exceeds 82% in the visible band. The results demonstrate that transparency and flexibility are the additional benefits that make the proposed absorber suitable for various potential applications.

Keywords: metamaterial absorber; optically transparent; flexible; silver nanowire; ultrathin



Citation: Dong, Y.; Yu, D.; Li, G.; Cao, Y.; Ruan, Y.; Lin, M. Ultrathin and Optically Transparent Microwave Absorber Based on Flexible Silver Nanowire Film. *Crystals* **2021**, *11*, 1583. <https://doi.org/10.3390/cryst11121583>

Academic Editors: Pooya Sareh, Yao Chen and George Kenanakis

Received: 25 November 2021

Accepted: 17 December 2021

Published: 19 December 2021

Publisher's Note: MDPI stays neutral with regard to jurisdictional claims in published maps and institutional affiliations.



Copyright: © 2021 by the authors. Licensee MDPI, Basel, Switzerland. This article is an open access article distributed under the terms and conditions of the Creative Commons Attribution (CC BY) license (<https://creativecommons.org/licenses/by/4.0/>).

1. Introduction

Over the past decades, microwave absorbers (MAs) have turned into one of the most thriving research topics in electromagnetic (EM) wave absorption technology [1,2], which is mainly due to EM radiation pollution. The conventional absorbers, such as the Salisbury screen [3], the Jaumann screen [4], and the pyramidal absorbers [5,6], cannot satisfy some application requirements because of the narrow absorption band or bulky structures. With the rapid development of metamaterials, the metamaterials microwave absorbers (MMAs) can achieve broadband, ultrathin, and perfect EM absorption [7] using a multi-resonant pattern [8,9], multi-layered [10,11] or lossy-component-loaded structures [12–14]. Generally, most of those MMAs are not optically transparent and cannot be applied in practical window applications.

Recently, broadband transparent metamaterials microwave absorbers (TMMAs) have been designed with different methods. A transparent EM wave absorption is usually achieved using transparent materials, such as oxide semiconductors [15,16], transparent metal coatings [17,18], and metal grid structures [19,20]. A broadband TMMMA using Al wire-grid has been designed as a sandwich structure [21], and its optical transmittance is less than 80%, which is affected by metal grid structures and thicker substrate. Indium tin oxide (ITO), chosen as the transparent material, has been designed to implement high transparency and broadband absorption at microwave frequencies by using different unit resonant patterns [22–28]. However, the TMMAs based on ITO have the disadvantages of high cost and limited mechanical flexibility. Moreover, graphene, as a new material with potential, has been envisaged as more suitable transparent material for TMMAs applications. However, for graphene-based TMMAs [29–34], it is difficult to fabricate for large areas and mass production. Therefore, there still are more efforts required to improve the absorption performances with thinner thickness, better light transmittance, and higher flexibility.

In this paper, we propose a flexible TMMA with ultrathin and broadband characteristics. The absorbing layer of patterned films is realized using silver nanowires (AgNWs) at a low cost. The model of absorber has been numerically simulated and experimentally verified, which attains broadband absorption with 80% absorptivity over 12 GHz, and thickness of less than $0.05\lambda_0$ (corresponding to a lower frequency). Meanwhile, the absorber is flexible and exhibits a wide-angle absorption performance for TE and TM waves. Compared with the reported absorbers, this design achieves optical transparency, high flexibility, broadband absorption, and ultrathin thickness at the same time.

2. Design and Methods

A schematic of the proposed optically transparent MA based on AgNWs is depicted in Figure 1. The unit cell has a sandwiched structure consisting of three layers: the top patterned AgNWs film, the space layer, and the bottom patterned AgNWs film. Both of the AgNWs films used in the structure are fabricated through the commercial standard process and enable the materials to have high optical transparency, and all the patterns are formed by laser etching [35–38]. The top pattern has a square-shaped split-ring slot. The four different-sized square patch slots are patterned on the bottom film, which is centrosymmetric in the unit cell. There is a space layer between the top and bottom films. The AgNWs coating thickness is about $0.24\ \mu\text{m}$ (values for different surface resistance). The silver nanowires ink is uniformly coated on the polyethylene terephthalate (PET). In the design process, these factors of optical transparency, thickness, and broadband absorption need to be considered simultaneously. In order to have a good impedance matching with free space, the top layer film needs to have high impedance characteristics (close to $377\ \Omega$). However, different from traditional high impedance surfaces (like mushroom, square patch), the square-shaped split-ring slot based on silver nanowires has the characteristics of ultra-thin and broadband resonance. In addition, to reduce the EM wave transmittance and increase the resonance intensity, the bottom layer adopts this pattern of four square patch slots with low resistance. Since silver nanowires and PET film will weaken the light transmittance of the absorber, the patterns of the top and bottom layers are both slot structures. The geometrical dimensions labelled in Figure 1 are as follows: $p = 13\ \text{mm}$, $n = 0.5\ \text{mm}$, $d = 2.15\ \text{mm}$, $m = 8\ \text{mm}$, $a = 2\ \text{mm}$, $b = 2.5\ \text{mm}$, $l = 2.5\ \text{mm}$.

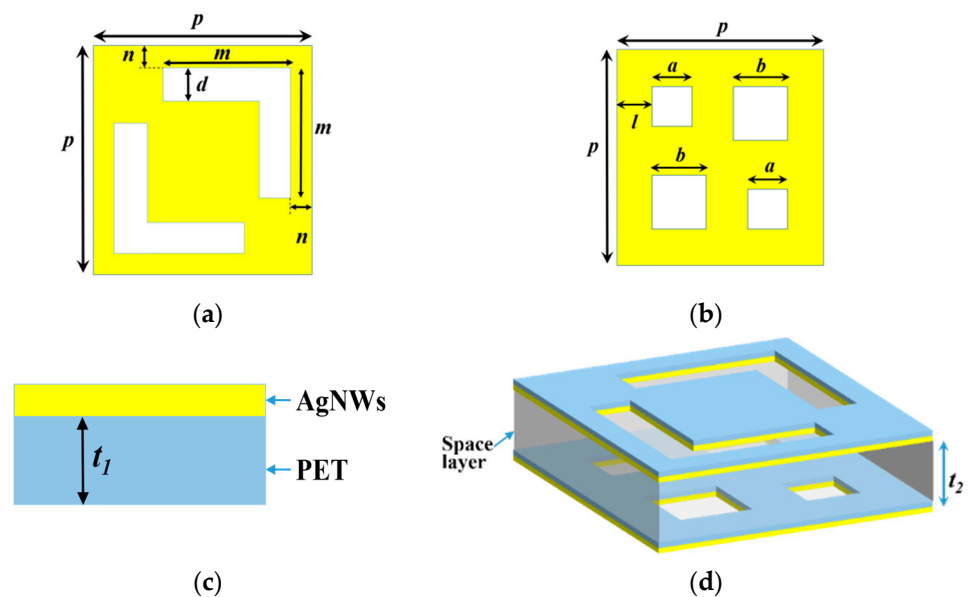


Figure 1. Schematic of the proposed absorber. (a) The top patterned silver nanowires (AgNWs) film. (b) The bottom patterned AgNWs film. (c) Cross-sectional view of the AgNWs film. (d) 3D view of the absorber.

To give physical insight into the absorption characteristics, we establish an equivalent circuit model (ECM) for the proposed absorber based on transmission line theory, as shown in Figure 2. The free-space impedance is Z_0 , and the permittivity of the air space is ϵ_0 . It can be assumed that the top and bottom pattern film are approximate to the RLC series circuits, and the corresponding impedances are denoted by Z_t and Z_b , respectively. The Z_s represents the space layer impedance, and the ϵ_0 and β_s are permittivity and propagation constants of the space layer, respectively.

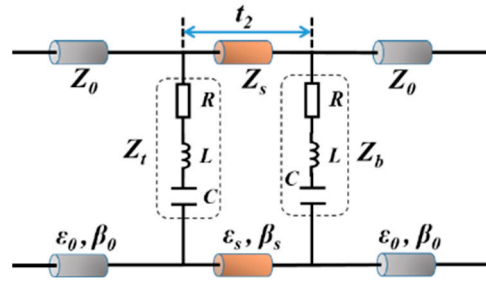


Figure 2. Equivalent circuit model (ECM) of the proposed absorber.

According to the two-port theory, the ABCD matrix of the structure is equal to

$$\begin{aligned} \begin{bmatrix} A & B \\ C & D \end{bmatrix} &= \begin{bmatrix} 1 & 0 \\ \frac{1}{Z_t} & 1 \end{bmatrix} \begin{bmatrix} \cos \beta_s t_2 & jZ_s \sin \beta_s t_2 \\ j\frac{\sin \beta_s t_2}{Z_s} & \cos \beta_s t_2 \end{bmatrix} \begin{bmatrix} 1 & 0 \\ \frac{1}{Z_b} & 1 \end{bmatrix} \\ &= \begin{bmatrix} \cos \beta_s t_2 + j\frac{Z_s}{Z_b} \sin \beta_s t_2 & jZ_s \sin \beta_s t_2 \\ \frac{Z_t + Z_b}{Z_t Z_b} \cos \beta_s t_2 + j\left(\frac{1}{Z_s} + \frac{Z_s}{Z_t Z_b}\right) \sin \beta_s t_2 & \cos \beta_s t_2 + j\frac{Z_s}{Z_t} \sin \beta_s t_2 \end{bmatrix} \end{aligned} \quad (1)$$

where t_2 is the thickness of the space layer, $Z_t = R_t + X_t$, and $Z_b = R_b + X_b$. Then, the reflection coefficient $|S_{11}|$ and transmission coefficient $|S_{21}|$ can also be expressed by matrix ABCD:

$$R = |S_{11}| = \left| \frac{A + B/Z_0 - CZ_0 - D}{A + B/Z_0 + CZ_0 + D} \right|, \quad (2)$$

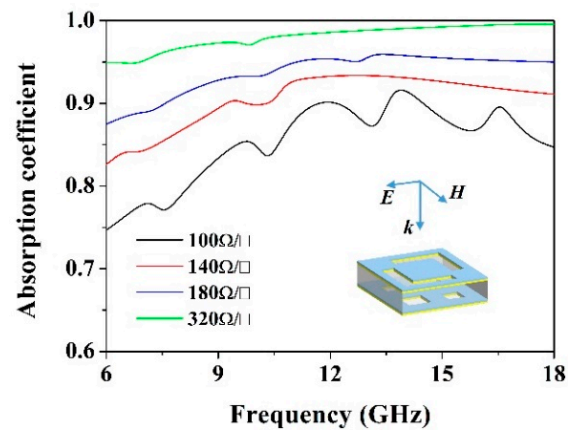
$$T = |S_{21}| = \left| \frac{2}{A + B/Z_0 + CZ_0 + D} \right| \quad (3)$$

where $A = \cos \beta_s t_2 + j\frac{Z_s}{Z_b} \sin \beta_s t_2$, $B = jZ_s \sin \beta_s t_2$, $C = \frac{Z_t + Z_b}{Z_t Z_b} \cos \beta_s t_2 + j\left(\frac{1}{Z_s} + \frac{Z_s}{Z_t Z_b}\right) \sin \beta_s t_2$, and $D = \cos \beta_s t_2 + j\frac{Z_s}{Z_t} \sin \beta_s t_2$. The absorption coefficient can be calculated as $A = 1 - R^2 - T^2$, where A is the coefficient of absorption power, R^2 is the coefficient of reflection power, and T^2 is the coefficient of transmission power. We consider that air is adopted as the spacer layer so that Z_s equals to Z_0 . Thus, it can be seen that the absorption performance depends on impedance Z_t and Z_b which is mainly related to the sheet resistance (R_t , R_b) and the equivalent reactance (X_t , X_b).

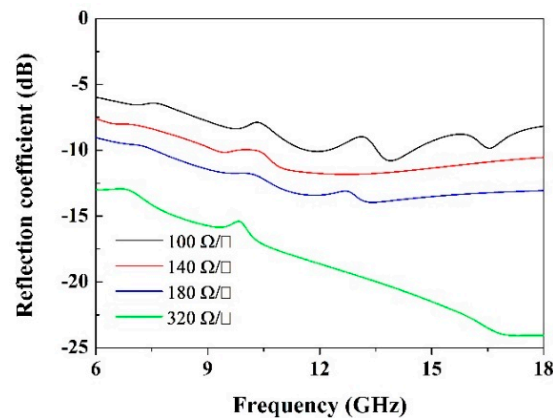
3. Results and Discussions

The proposed TMMA was performed in commercial software CST based on the finite integration method. During the numerical simulation, the mesh number of the designed model is 13635, and four processor cores (CPU, Core i7-6700) and 16,800 MB of memory (RAM) have been used, which results in the total calculation time of 1 min. In order to simulate the periodic array structure, the unit-cell boundary condition was set in the software. The space layer is regarded as air spacer with the thickness of $t_2 = 2$ mm, and the PET sheet ($\epsilon_r = 3.6$, $\tan \delta = 0.003$) has a thickness (t_1) of 0.125 mm. The sheet resistance of the top film is $R_t = 320 \Omega/\text{square}$, $180 \Omega/\text{square}$, $140 \Omega/\text{square}$, $100 \Omega/\text{square}$. Additionally, the bottom films R_b keep constant and equal to $28 \Omega/\text{square}$. The other parameters are the same as previously mentioned. The simulation result is shown in Figure 3 for normal incidence. It is observed that with increasing top film resistance, the

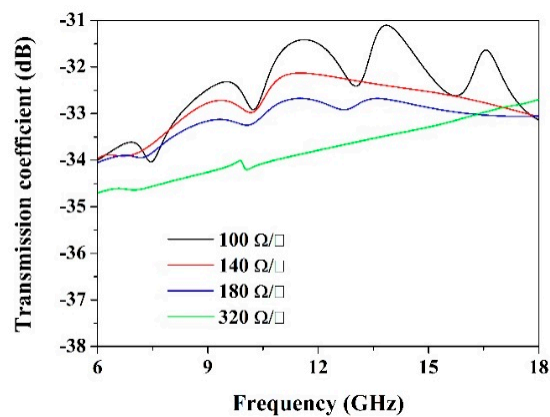
absorption performance in the frequency range of 6 GHz–18 GHz is gradually enhanced. The absorption coefficient curve gradually moves higher as the frequency increases, as same as the reflection coefficient. When $R_t = 320 \Omega/\text{square}$, the absorption coefficient is greater than 0.9, which can achieve near-perfect absorbance in a wide frequency range. It can be concluded that the impedance of the absorber is perfectly matched with the free-space impedance Z_0 over the whole band. Besides, regardless of the value of top film impedance, EM waves are barely transmitted.



(a)



(b)



(c)

Figure 3. Absorption coefficients and reflection/transmission coefficients. (a) Absorption coefficients. (b) Reflection coefficients. (c) Transmission coefficients.

The absorption spectra under the incident EM wave with different angles θ are also investigated, as shown in Figure 4. In transverse electric (TE) mode, when the incident angle varies from 0° to 50° , the absorbing strength weakens slightly, but the absorption bandwidth ($A > 0.8$) remains almost the same. Note that the higher the frequency, the less affected by the incident angle. In the case of transverse magnetic (TM) mode, although the absorbing band has a slight decrease with increasing incident angle, the absorption is moderately affected by the different incident angles, which invariably keeps high efficiency. This could be due to the fact that the magnetic field component parallel to the top film decreases as the angle of incidence tends to be parallel. Therefore, it can be noted that the proposed TMMA reveals a wide-angle absorption performance for both the TE and TM modes.

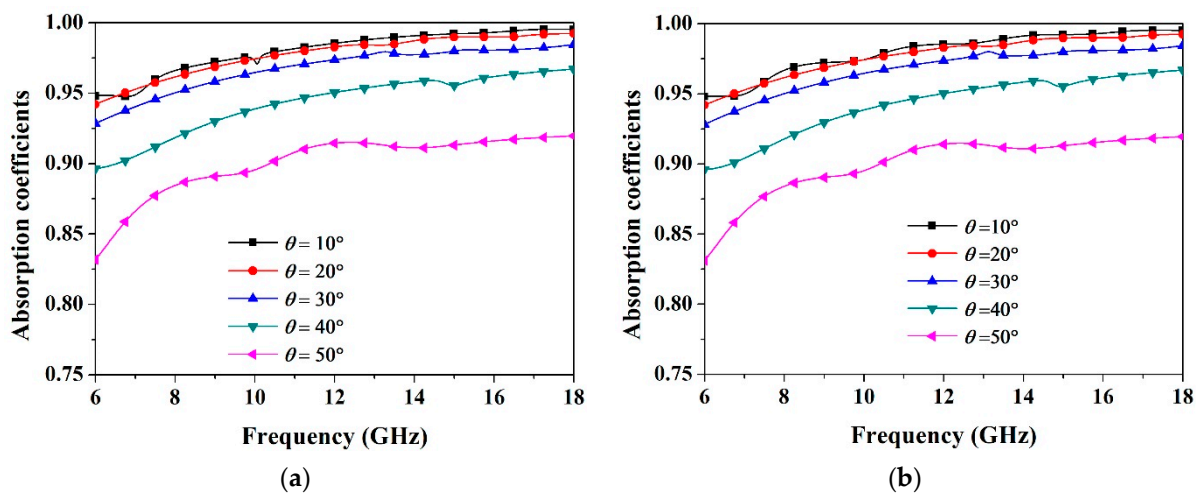


Figure 4. Absorption coefficients for oblique incidence θ . (a) TE mode. (b) TM mode.

To further excavate the physical mechanism of broadband absorption characteristics, the distributions of electric field and surface current have been investigated in Figures 5 and 6. At the frequency of 6 GHz, the electric field is mainly concentrated on both edges and corners of the square split-ring, resulting in a capacitive effect between adjacent units. At the higher frequency, most electric fields are focused on both the inner and gap of the square split-ring, which leads to stronger localization of the electric field. In Figure 6, we can observe that the top surface current is gathered at the edge of the square split-ring at a lower frequency, whereas the current densities in the central region gradually rise with increasing frequency. The current flow on the top and bottom layers are parallel in the same direction, which indicates that there is a strong electric resonance. Compared with the bottom layer, the electric field and surface current are mainly distributed in the top layer. This means that the power of the incident wave is mainly dissipated on the top layer due to the ohmic loss caused by electric resonance.

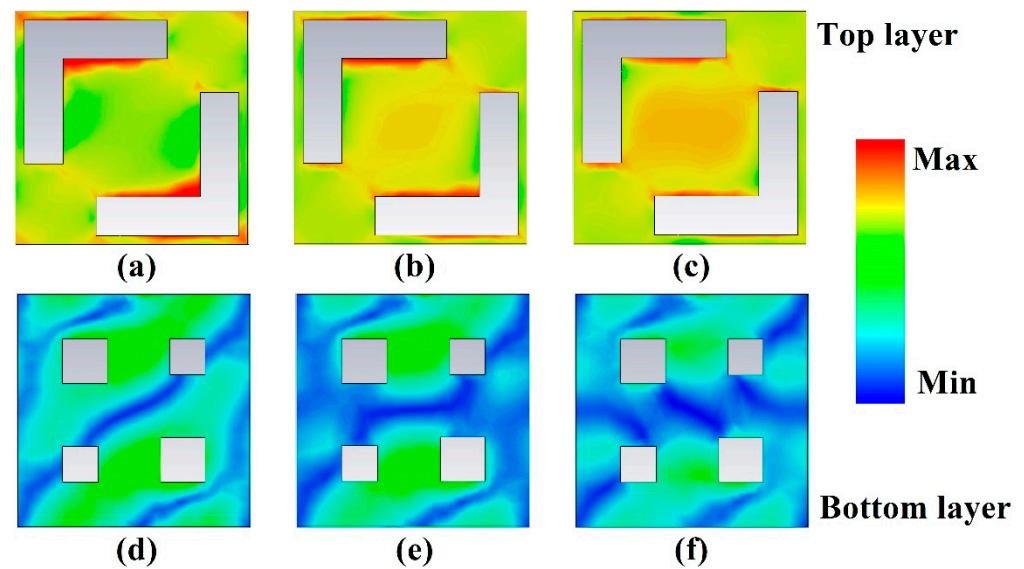


Figure 5. The magnitude distribution of electric field on top and bottom films at different frequencies. (a–c) The magnitude distribution of electric field at 6GHz, 12 GHz and 18 GHz on top layer. (d–f) The magnitude distribution of electric field at 6GHz, 12 GHz and 18 GHz on bottom layer.

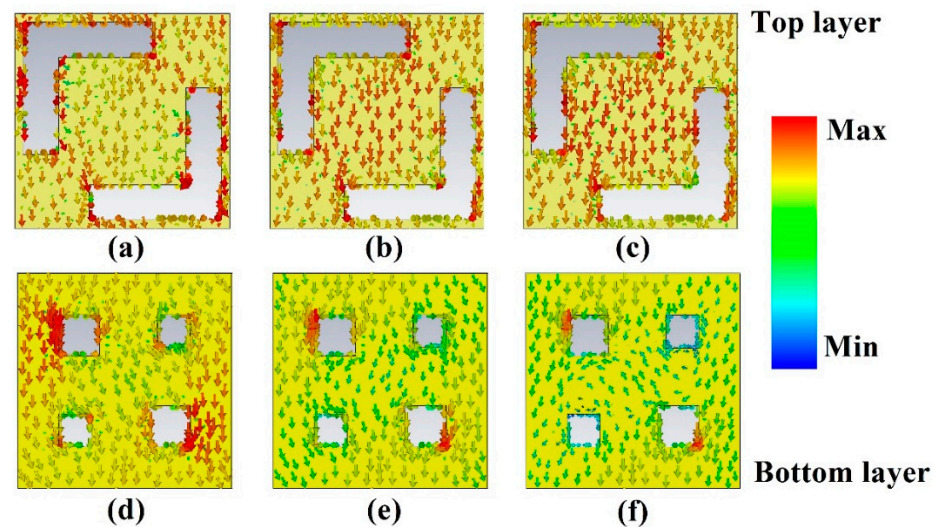


Figure 6. The distribution of surface currents on top and bottom films at different frequencies. (a–c) The distribution of surface currents at 6GHz, 12 GHz and 18 GHz on top layer. (d–f) The distribution of surface currents at 6GHz, 12 GHz and 18 GHz on bottom layer.

4. Experiments

To validate the absorption performance, the proposed absorber composed of 22×22 unit cells is fabricated with the overall size of $286 \text{ mm} \times 286 \text{ mm}$. For the top and bottom layer, AgNWs films are coated on the 0.125 mm PET films, and the sheet resistances of the top and bottom film are about $320 \text{ } \Omega/\text{square}$ and $28 \text{ } \Omega/\text{square}$, respectively. Both PET and silver nanowires are etched into the designed pattern by laser etching. The concentration of AgNWs ink (viscosity: 7.34 cP , tension: 41.522 mN/m) used is 0.392% . The diameter and length of silver nanowires are $20\text{--}25 \text{ nm}$ and $30\text{--}35 \mu\text{m}$. The ink coating is carried out with a Slot Die Coater (SHINING, Shenzhen, PR China). The whole coating process consists of loading material, coating, ultraviolet curing, and laminating. The drying process adopts staged drying, and the drying temperatures are $75 \text{ }^\circ\text{C}$, $95 \text{ }^\circ\text{C}$, $120 \text{ }^\circ\text{C}$, $100 \text{ }^\circ\text{C}$, and $60 \text{ }^\circ\text{C}$. The laser etching is implemented by a CO_2 laser (50W , one pulse). The spot size of the laser is $100 \mu\text{m}$. For the whole sample, the total laser etching time is $25\text{--}40 \text{ min}$.

The photograph of the sample shown in Figure 7 has good optical transparency. The average optical transmittance (380 nm–760 nm) is more than 82% through testing the different positions of the whole structure. The top film and bottom film are inserted into a double layer of square ring paperboard (a single layer of square ring paperboard has a thickness of 1.007 mm), meeting the requirements of a 2 mm-thick air spacer. The measured total thickness of the clamp and absorber is 4.555 mm. After subtracting the thickness of the front and back cardboard clamp (the thickness of the clamp is the same as square ring paperboard), the thickness of the absorber is 2.541 mm.

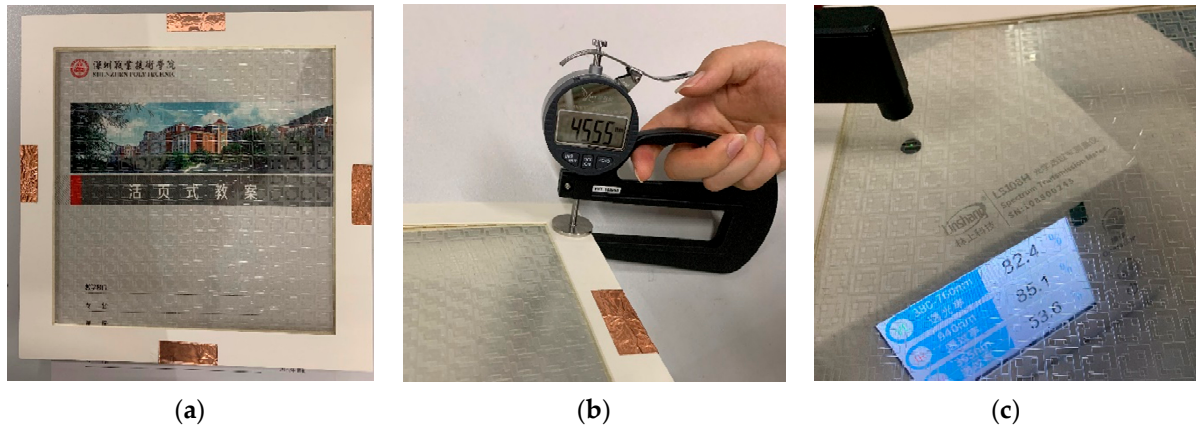


Figure 7. Measurement of thickness and optical transmittance for fabricated sample. (a) Fabricated sample. (b) Thickness measurement. (c) Optical transmittance measurement.

The absorption experiment is carried out in an anechoic chamber using the free space method. Two standard wideband horn antennas (1 GHz–18 GHz) connected to the vector network analyzer (VNA, Advantest R3770) are regarded as the transmitter and receiver, and both the antennas should aim at the center of the sample, as shown in Figure 8. In the case of reflection measurement, a flat metallic board is used as the reference reflection plane. Two horn antennas are placed on the same side of the sample. In the case of transmission measurement, the air window is used as the reference transmission plane, and the horn antennas are respectively placed on both sides of the sample and in the same line. The measured absorption spectrum is depicted in Figure 9. Compared with the simulation results, the measured absorption exhibits good coincidence from 9 GHz–15 GHz. The slight difference observed from the comparison is mainly due to the following reasons: (1) the fabrication error of the AgNWs films; (2) the slight bending of the sample in the measurement; (3) the mutual coupling effect of two horn antenna in the low-frequency band.

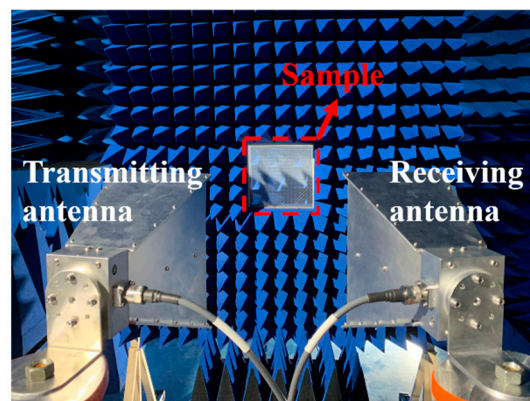


Figure 8. Measurement setup.

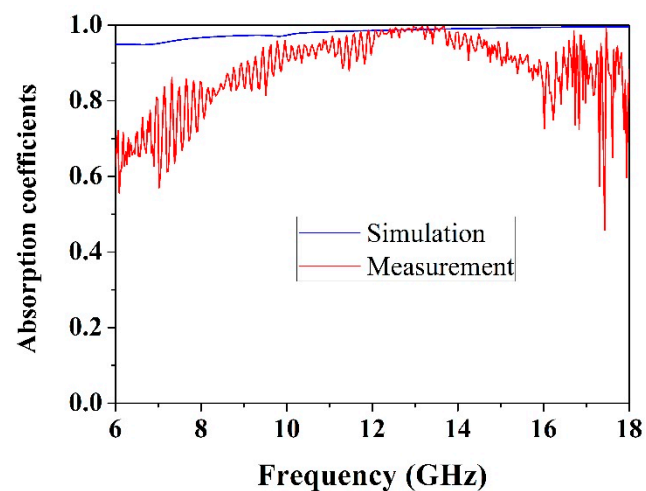


Figure 9. Simulated and measured absorption spectrum of the AgNWs-based transparent metamaterials microwave absorber (TMMA).

5. Conclusions

In summary, a flexible and transparent microwave absorber with an ultrathin thickness has been proposed, using AgNWs film. The absorption principle based on the effective-medium method and the transmission line theory has been illustrated. The proposed absorber exhibits an excellent absorption bandwidth (6 GHz~18 GHz) with high absorption coefficients above 0.8, and the experimental results basically agree with that of the simulated result. The fabricated absorber has a measured optical transmittance of 82% in the visible band (380 nm–760 nm). Meanwhile, this structure has a good angular stability with the oblique incidence angle (up to 50°) for both TE and TM modes. The designed absorber is particularly promising for applications in the area of intelligent wearable devices, window EM protection, and stealth technology.

Author Contributions: This study was conducted through the contributions of all authors. Conceptualization, investigation, validation, writing—original draft preparation, D.Y. and Y.D.; software, writing—review and editing, G.L. and M.L.; visualization, supervision, Y.C. and Y.R. All authors have read and agreed to the published version of the manuscript.

Funding: This work was supported by the Equipment Advance Research Field Fund Project under Grant No. 80909010205.

Institutional Review Board Statement: Not applicable.

Informed Consent Statement: Not applicable.

Data Availability Statement: Not applicable.

Conflicts of Interest: The authors declare no conflict of interest.

References

1. Turkey, M.M.; Gupta, N. Electromagnetic absorber design challenges. *IEEE Electromagn. Compat. Mag.* **2019**, *8*, 59–65. [[CrossRef](#)]
2. Bakır, M.; Karaaslan, M.; Unal, E.; Akgol, O.; Sabah, C. Microwave metamaterial absorber for sensing applications. *Opto-Electron. Rev.* **2017**, *25*, 318–325. [[CrossRef](#)]
3. Salisbury, W.W. Absorbent body of electromagnetic waves. U.S. Patent 2,599,944, 10 June 1952.
4. Du Toit, L.J. The design of Jauman absorbers. *IEEE Antennas Propag. Mag.* **1994**, *36*, 17–25. [[CrossRef](#)]
5. Park, M.J.; Choi, J.; Kim, S.S. Wide bandwidth pyramidal absorbers of granular ferrite and carbonyl iron powders. *IEEE Trans. Magn.* **2000**, *36*, 3272–3274. [[CrossRef](#)]
6. Naito, Y.; Suetake, K. Application of ferrite to electromagnetic wave absorber and its characteristics. *IEEE Trans. Microw. Theory Tech.* **1971**, *19*, 65–72. [[CrossRef](#)]
7. Ali, S.A.M.; Abu, M.; Zabri, S.N. A review: The development of metamaterial absorber. *Int. J. Integr. Eng.* **2020**, *12*, 72–80.
8. Li, L.; Lv, Z. Ultra-wideband polarization-insensitive and wide-angle thin absorber based on resistive metasurfaces with three resonant modes. *J. Appl. Phys.* **2017**, *122*, 055104. [[CrossRef](#)]

9. Machado, G.G.; Cahill, R.; Fusco, V.; Conway, G. Comparison of FSS topologies for maximising the bandwidth of ultra-thin microwave absorbers. In Proceedings of the 13th European Conference on Antennas and Propagation (EuCAP), Krakow, Poland, 31 March–5 April 2019; pp. 1–5.
10. Soheilifar, M.R.; Sadeghzadeh, R.A. Design, fabrication and characterisation of scaled and stacked layers planar metamaterial absorber. *IET Microw. Antennas Propag.* **2015**, *9*, 86–93. [[CrossRef](#)]
11. Zhang, Z.; Zhang, L.; Chen, X.; Wu, Z.; He, Y.; Lv, Y.; Zou, Y. Broadband metamaterial absorber for low-frequency microwave absorption in the S-band and C-band. *J. Magn. Magn. Mater.* **2020**, *497*, 166075. [[CrossRef](#)]
12. Fang, J.; Huang, J.; Gou, Y.; Shang, Y. Research on broadband tunable metamaterial absorber based on PIN diode. *Optik* **2020**, *200*, 163171. [[CrossRef](#)]
13. Zhu, J.; Li, D.; Yan, S.; Cai, Y.; Liu, Q.H.; Lin, T. Tunable microwave metamaterial absorbers using varactor-loaded split loops. *Europhys. Lett.* **2015**, *112*, 54002. [[CrossRef](#)]
14. Chang, Y.; Wei, J.; Lee, C. Metamaterials—from fundamentals and MEMS tuning mechanisms to applications. *Nanophotonics* **2020**, *9*, 3049–3070. [[CrossRef](#)]
15. Jayathilake, D.; Peiris, T.N. Overview on transparent conducting oxides and state of the art of low-cost doped ZnO systems. *SF J. Mater. Chem Eng.* **2018**, *1*, 1004.
16. Li, X.; Wang, L.; Li, X.; Zhang, J.; Wang, M.; Che, R. Multi-dimensional ZnO@MWCNTs assembly derived from MOF-5 heterojunction as highly efficient microwave absorber. *Carbon* **2021**, *172*, 15–25. [[CrossRef](#)]
17. Li, W.; Shamim, A. Silver Nanowires Based Transparent, Broadband FSS Microwave Absorber. In Proceedings of the 13th European Conference on Antennas and Propagation (EuCAP), Krakow, Poland, 31 March–5 April 2019; pp. 1–3.
18. Okano, Y.; Ogino, S.; Ishikawa, K. Development of optically transparent ultrathin microwave absorber for ultrahigh-frequency RF identification system. *IEEE Trans. Microw. Theory Tech.* **2012**, *60*, 2456–2464. [[CrossRef](#)]
19. Wu, Y.; Fu, C.; Qian, S.; Zong, Z.; Wu, X.; Yue, Y.; Gu, W. Flexible and transparent W-band absorber fabricated by EHD printing technology. *IEEE Antennas Wirel. Propag. Lett.* **2020**, *19*, 1345–1349. [[CrossRef](#)]
20. Min, P.; Song, Z.; Yang, L.; Dai, B.; Zhu, J. Transparent ultrawideband absorber based on simple patterned resistive metasurface with three resonant modes. *Opt. Express* **2020**, *28*, 19518–19530. [[CrossRef](#)] [[PubMed](#)]
21. Jang, T.; Youn, H.; Shin, Y.J.; Guo, L.J. Transparent and flexible polarization-independent microwave broadband absorber. *ACS Photonics* **2014**, *1*, 279–284. [[CrossRef](#)]
22. Sheokand, H.; Singh, G.; Ghosh, S.; Ramkumar, J.; Ramakrishna, S.A.; Srivastava, K.V. An optically transparent broadband microwave absorber using interdigital capacitance. *IEEE Antennas Wirel. Propag. Lett.* **2018**, *18*, 113–117. [[CrossRef](#)]
23. Chen, L.; Ruan, Y.; Luo, S.S.; Ye, F.J.; Cui, H.Y. Optically Transparent Metasurface Absorber Based on Reconfigurable and Flexible Indium Tin Oxide Film. *Micromachines* **2020**, *11*, 1032. [[CrossRef](#)]
24. Shen, Y.; Zhang, J.; Pang, Y.; Wang, J.; Ma, H.; Qu, S. Transparent broadband metamaterial absorber enhanced by water-substrate incorporation. *Opt. Express* **2018**, *26*, 15665–15674. [[CrossRef](#)] [[PubMed](#)]
25. Zhou, Q.; Yin, X.; Ye, F.; Mo, R.; Tang, Z.; Fan, X.; Cheng, L.; Zhang, L. Optically transparent and flexible broadband microwave metamaterial absorber with sandwich structure. *Appl. Phys. A* **2019**, *125*, 131. [[CrossRef](#)]
26. Zheng, Y.; Chen, K.; Jiang, T.; Zhao, J.; Feng, Y. Multi-octave microwave absorption via conformal metamaterial absorber with optical transparency. *J. Phys. D Appl. Phys.* **2019**, *52*, 335101. [[CrossRef](#)]
27. Deng, R.; Zhang, K.; Li, M.; Song, L.; Zhang, T. Targeted design, analysis and experimental characterization of flexible microwave absorber for window application. *Mater. Des.* **2019**, *162*, 119–129. [[CrossRef](#)]
28. Lai, S.; Wu, Y.; Zhu, X.; Gu, W.; Wu, W. An optically transparent ultrabroadband microwave absorber. *IEEE Photonics J.* **2017**, *9*, 5503310. [[CrossRef](#)]
29. Lu, W.B.; Wang, J.W.; Zhang, J.; Liu, Z.; Chen, H.; Song, W.; Jiang, Z. Flexible and optically transparent microwave absorber with wide bandwidth based on graphene. *Carbon* **2019**, *152*, 70–76. [[CrossRef](#)]
30. Yi, D.; Wei, X.C.; Xu, Y.L. Transparent microwave absorber based on patterned graphene: Design, measurement, and enhancement. *IEEE Trans. Nanotechnol.* **2017**, *16*, 484–490. [[CrossRef](#)]
31. Wu, B.; Tuncer, H.M.; Naeem, M.; Yang, B.; Cole, M.T.; Milne, W.I.; Hao, Y. Experimental demonstration of a transparent graphene millimetre wave absorber with 28% fractional bandwidth at 140 GHz. *Sci. Rep.* **2014**, *4*, 4130. [[CrossRef](#)]
32. Yi, D.; Wei, X.C.; Xu, Y.L. Tunable microwave absorber based on patterned graphene. *IEEE Trans. Microw. Theory Tech.* **2017**, *65*, 2819–2826. [[CrossRef](#)]
33. Grande, M.; Bianco, G.V.; Vincenti, M.A.; De Ceglia, D.; Capezzuto, P.; Petruzzelli, V.; Scalora, M.; Bruno, G.; D’Orazio, A. Optically transparent microwave screens based on engineered graphene layers. *Opt. Express* **2016**, *24*, 22788–22795. [[CrossRef](#)]
34. Lu, Z.; Ma, L.; Tan, J.; Wang, H.; Ding, X. Transparent multi-layer graphene/polyethylene terephthalate structures with excellent microwave absorption and electromagnetic interference shielding performance. *Nanoscale* **2016**, *8*, 16684–16693. [[CrossRef](#)]
35. Yang, C.; Gu, H.; Lin, W.; Yuen, M.M.; Wong, C.P.; Xiong, M.; Gao, B. Silver nanowires: From scalable synthesis to recyclable foldable electronics. *Adv. Mater.* **2011**, *23*, 3052–3056. [[CrossRef](#)] [[PubMed](#)]
36. Yang, P.A.; Huang, Y.; Li, R.; Huang, X.; Ruan, H.; Shou, M.; Li, W.; Zhang, Y.; Li, N.; Dong, L. Optimization of Fe@Ag core-shell nanowires with improved impedance matching and microwave absorption properties. *Chem. Eng. J.* **2022**, *430*, 132878. [[CrossRef](#)]

-
37. Yu, S.; Ma, X.; Li, X.; Li, J.; Gong, B.; Wang, X. Enhanced adhesion of Ag nanowire based transparent conducting electrodes for application in flexible electrochromic devices. *Opt. Mater.* **2021**, *120*, 111414. [[CrossRef](#)]
 38. Ran, Y.; He, W.; Wang, K.; Ji, S.; Ye, C. A one-step route to Ag nanowires with a diameter below 40 nm and an aspect ratio above 1000. *Chem. Commun.* **2014**, *50*, 14877–14880. [[CrossRef](#)] [[PubMed](#)]